Available online at www.sciencedirect.com

ScienceDirect

Journal of the Franklin Institute 351 (2014) 4817–4837

Journal of The Franklin Institute

www.elsevier.com/locate/jfranklin

An adaptive controller for nonlinear teleoperators with variable time-delays ☆

Ioannis Sarras[a], Emmanuel Nuño[b,*], Luis Basañez[c]

[a]Automatic Control Department, SUPELEC, Gif-sur-Yvette, France
[b]Department of Computer Science, CUCEI, University of Guadalajara, Guadalajara, Mexico
[c]Institute of Industrial and Control Engineering, Technical University of Catalonia, Barcelona, Spain

Received 8 October 2013; received in revised form 12 May 2014; accepted 30 July 2014
Available online 9 August 2014

Abstract

In most real-life bilateral teleoperators the available physical parameters are uncertain and the communications exhibit variable time-delays. In order to confront these situations and only assuming that a bound of the time-delays is known, the present work reports an adaptive controller which ensures asymptotic convergence of both position errors and velocities to zero, provided that a sufficient condition on the control gains is met. Compared to previous related works that only treated constant time-delays, the stability analysis does not rely on the *cascade interconnection* structure of the local and remote nonlinear dynamics and the linear interconnection map. Instead, the paper employs a different Lyapunov candidate function that incorporates a strictly positive term, the local and remote position error. Some simulations, in free space and interacting with a rigid wall, and experiments, using two nonlinear manipulators, illustrate the performance of the proposed control scheme in the presence of uncertain parameters and variable time-delays.

1. Introduction

The control of bilateral teleoperators is a highly active field, that is challenging due to the complexity of their nonlinear dynamics, to the time-delays in the communications as well as to

☆This work has been partially supported by the Mexican projects CONACyT CB-129079 and INFR-229696 and the Spanish CICYT projects DPI2010-15446 and DPI2011-22471.

*Corresponding author. Tel.: +52 33 13785900x27748.
E-mail addresses: sarras@ieee.org (I. Sarras), emmanuel.nuno@cucei.udg.mx (E. Nuño), luis.basanez@upc.edu (L. Basañez).

http://dx.doi.org/10.1016/j.jfranklin.2014.07.016
0016-0032/

their wide range of practical real-life applications. A major breakthrough to the treatment of this problem has been the use of scattering signals (wave variables) to transform the pure time-delay communication channel into a passive transmission line. Assuming that the human operator and the environment are passive (from force to velocity) and using a damping injection term on the local and the remote manipulators' controllers to transform the passive mechanical manipulators into output strictly passive systems, asymptotic convergence to zero of velocities can be ensured [1,2]. For a historical survey along this research line the reader may refer to [3] and, for a tutorial on teleoperators control, to [4].

Position tracking is rarely ensured by scattering-based schemes mostly because the communications lose their passive behavior, if a position error term is added in the controller, due to the extra energy generated by such term [5]. PD-like schemes that overcome this obstacle, and that do not employ the scattering transformation, have been reported in [6–8]. The authors in [9] proposed to formulate the position tracking problem in terms of synchronization, which also avoids the scattering transformation. An adaptive version of this scheme is proposed in [10] where the aim is to synchronize the local and remote positions and velocities using a synchronizing signal that is a linear combination of such positions and velocities.

In [11] an adaptive controller is reported for uncertain bilateral teleoperators with constant time-delays capable of ensuring asymptotic convergence to zero of both, local and remote, position errors and velocities. The main, simple but essential, difference between the controller in [11] and the one in [10] is the use of a linear combination of the velocity and the position error—instead only of the position—in the, so-called, synchronizing signal. This idea has been latter ported in [12] to the synchronization and consensus problem of networks of nonidentical Euler–Lagrange systems. It is worth mentioning that, up to the authors knowledge, the robustness property of the adaptive controllers has not been ported to the teleoperators control with variable time-delays (a nice exception is the recent work [13], where an adaptive controller together with a high-gain sliding term is proposed. However, a high-gain is never desirable in practical applications).

Motivated by the wide number of applications of bilateral teleoperators that exhibit variable time-delays in their communications [14–16], the present paper reports an extension to the variable time-delays case of the controller of [11]. It should be underscored that the proof of the convergence in [11] relies on the analysis of a *cascade interconnection* between the nonlinear dynamics of the local and remote manipulators and a linear map that accounts for their interconnection and contains some time-delayed terms, with the synchronizing signal as an input. The linear map stability is studied in the frequency domain using the Laplace transform [17]. Clearly, such technique cannot be employed in the case of variable time-delays. Instead, this proposal employs a different Lyapunov function candidate that incorporates a strictly positive term: the local and remote position error. The main contribution of the present work is a novel sufficient condition for the asymptotic convergence of both position errors and velocities to zero provided that a bound of the time-delays is known and the human operator and environment forces are zero. Simulations and experiments in free space and in contact with a rigid environment are presented to evidence the performance of the proposed approach. Compared to [18], this paper also analyzes the teleoperator stability properties when the human operator and environment forces are not zero and validates the control proposal with some experiments.

To streamline the presentation, throughout the paper the following *notation* is introduced. Italic lower case letters denote scalar functions, *e.g.* t, bold lower case letters denote vectors, *e.g.* $\mathbf{x}$, and bold upper case letters denote matrices, *e.g.* $\mathbf{A}$. Moreover, $\mathbf{I}$, $\varnothing$ will be the identity and all-zero matrices, respectively, of appropriate dimensions. Additionally, we define $\mathbb{R}:=(-\infty,\infty)$,

$\mathbb{R}_{>0} := (0, \infty)$, $\mathbb{R}_{\geq 0} := [0, \infty)$. $\lambda_m\{\mathbf{A}\}$ and $\lambda_M\{\mathbf{A}\}$ represent the minimum and maximum eigenvalues of matrix $\mathbf{A}$, respectively, while $\|\mathbf{A}\|$ denotes the matrix-induced 2-norm. $|\mathbf{x}|$ stands for the standard Euclidean norm of vector $\mathbf{x}$. For any function $\mathbf{f} : \mathbb{R}_{\geq 0} \to \mathbb{R}^n$, the $\mathcal{L}_\infty$-norm is defined as $\|\mathbf{f}\|_\infty := \sup_{t \geq 0} |\mathbf{f}(t)|$, and the $\mathcal{L}_2$-norm as $\|\mathbf{f}\|_2 := (\int_0^\infty |\mathbf{f}(t)|^2 \, dt)^{1/2}$. The $\mathcal{L}_\infty$ and $\mathcal{L}_2$ spaces are defined as the sets $\{\mathbf{f} : \mathbb{R}_{\geq 0} \to \mathbb{R}^n : \|\mathbf{f}\|_\infty < \infty\}$ and $\{\mathbf{f} : \mathbb{R}_{\geq 0} \to \mathbb{R}^n : \|\mathbf{f}\|_2 < \infty\}$, respectively.

2. Background

This section reviews the dynamical model of the nonlinear bilateral teleoperator and the previous adaptive controller.

2.1. Nonlinear dynamical model

The local and remote robot manipulators are modeled as a pair of n-Degree Of Freedom (DOF), fully actuated, Euler–Lagrange systems [19]. Their corresponding nonlinear dynamics are given by

$$\begin{aligned} \mathbf{M}_l(\mathbf{q}_l)\ddot{\mathbf{q}}_l + \mathbf{C}_l(\mathbf{q}_l, \dot{\mathbf{q}}_l)\dot{\mathbf{q}}_l + \mathbf{g}_l(\mathbf{q}_l) &= \boldsymbol{\tau}_h - \boldsymbol{\tau}_l \\ \mathbf{M}_r(\mathbf{q}_r)\ddot{\mathbf{q}}_r + \mathbf{C}_r(\mathbf{q}_r, \dot{\mathbf{q}}_r)\dot{\mathbf{q}}_r + \mathbf{g}_r(\mathbf{q}_r) &= \boldsymbol{\tau}_r - \boldsymbol{\tau}_e, \end{aligned} \tag{1}$$

where $\ddot{\mathbf{q}}_i, \dot{\mathbf{q}}_i, \mathbf{q}_i \in \mathbb{R}^n$ are the acceleration, velocity and joint position, respectively. The subscript $i = \{l, r\}$ refers to the local and remote manipulators, respectively. The mapping $\mathbf{M}_i : \mathbb{R}^n \to \mathbb{R}^{n \times n}$ is the inertia matrix; $\mathbf{C}_i : \mathbb{R}^n \times \mathbb{R}^n \to \mathbb{R}^{n \times n}$ is the Coriolis and centrifugal effects matrix, defined via the Christoffel symbols of the first kind; $\mathbf{g}_i : \mathbb{R}^n \to \mathbb{R}^n$ is the vector of gravitational forces; $\boldsymbol{\tau}_i \in \mathbb{R}^n$ is the control signal and $\boldsymbol{\tau}_h \in \mathbb{R}^n$, $\boldsymbol{\tau}_e \in \mathbb{R}^n$ are the joint torques corresponding to the forces exerted by the human operator and the environment interaction, respectively [19,20].

With regard to the dynamics (1), the following standard assumption is adopted:

A1. The generalized inertia matrix is positive definite and bounded, i.e., $\forall \mathbf{q}$, $m_m^i \mathbf{I} \leq \mathbf{M}_i(\mathbf{q}) \leq m_M^i \mathbf{I}$, where $m_m^i := \lambda_m\{\mathbf{M}_i(\mathbf{q})\}$ and $m_M^i := \lambda_M\{\mathbf{M}_i(\mathbf{q})\}$.

Further, it is well known that dynamics (1) enjoy the following properties [20,21,8]:

P1. Matrix $\dot{\mathbf{M}}_i(\mathbf{q}_i) - 2\mathbf{C}_i(\mathbf{q}_i, \dot{\mathbf{q}}_i)$ is skew-symmetric.

P2. For all $\mathbf{q}, \mathbf{x} \in \mathbb{R}^n$, $\exists k_c^i \in \mathbb{R}_{>0}$ such that $|\mathbf{C}_i(\mathbf{q}, \mathbf{x})\mathbf{x}| \leq k_c^i |\mathbf{x}|^2$.

P3. The dynamics is linearly parameterizable such that, for all $\mathbf{x}, \mathbf{y} \in \mathbb{R}^n$, $\mathbf{M}_i(\mathbf{q}_i)\mathbf{y} + \mathbf{C}_i(\mathbf{q}_i, \dot{\mathbf{q}}_i)\mathbf{x} + \mathbf{g}_i(\mathbf{q}_i) = \mathbf{Y}_i(\mathbf{q}_i, \dot{\mathbf{q}}_i, \mathbf{x}, \mathbf{y})\boldsymbol{\theta}_i$, where $\mathbf{Y}_i \in \mathbb{R}^{n \times p}$ is a map of known functions and $\boldsymbol{\theta}_i \in \mathbb{R}^p$ is a constant vector with the manipulator physical parameters (link masses, moments of inertia, etc.).

2.2. Previous approach for constant time-delays

Let $\mathbf{e}_i \in \mathbb{R}^n$ denote the position errors, defined, for a constant time-delay T, by

$$\mathbf{e}_l := \mathbf{q}_l - \mathbf{q}_r(t - T); \quad \mathbf{e}_r := \mathbf{q}_r - \mathbf{q}_l(t - T). \tag{2}$$

The control objective of [11] is to drive the position errors and the velocities to zero independently of the constant time-delay T and without using the scattering transformation.

The following adaptive controllers are used

$$\boldsymbol{\tau}_l = \lambda\hat{\mathbf{M}}_l(\mathbf{q}_l)\dot{\mathbf{e}}_l + \lambda\hat{\mathbf{C}}_l(\mathbf{q}_l,\dot{\mathbf{q}}_l)\mathbf{e}_l - \hat{\mathbf{g}}_l(\mathbf{q}_l) + \mathbf{K}_l\boldsymbol{\epsilon}_l + \mathbf{B}\dot{\mathbf{e}}_l$$
$$\boldsymbol{\tau}_r = -\lambda\hat{\mathbf{M}}_r(\mathbf{q}_r)\dot{\mathbf{e}}_r - \lambda\hat{\mathbf{C}}_r(\mathbf{q}_r,\dot{\mathbf{q}}_r)\mathbf{e}_r + \hat{\mathbf{g}}_r(\mathbf{q}_r) - \mathbf{K}_r\boldsymbol{\epsilon}_r - \mathbf{B}\dot{\mathbf{e}}_r, \tag{3}$$

where $\hat{\mathbf{M}}_i(\mathbf{q}_i)$, $\hat{\mathbf{C}}_i(\mathbf{q}_i,\dot{\mathbf{q}}_i)$ and $\hat{\mathbf{g}}_i(\mathbf{q}_i)$ are the estimation of the inertia matrix, the Coriolis matrix and the gravity vector, respectively. The controller gains $\mathbf{K}_i$ and $\mathbf{B}$ are diagonal and positive definite $n\times n$ matrices. Additionally, the synchronizing signal $\boldsymbol{\epsilon}_i$ is defined as

$$\boldsymbol{\epsilon}_i := \dot{\mathbf{q}}_i + \lambda\mathbf{e}_i, \tag{4}$$

for any $\lambda\in\mathbb{R}_{>0}$.

Using property P3, with $\mathbf{Y}_i\hat{\boldsymbol{\theta}}_i = \lambda\hat{\mathbf{M}}_i\dot{\mathbf{e}}_i + \lambda\hat{\mathbf{C}}_i\mathbf{e}_i - \hat{\mathbf{g}}_i$, controllers (3) can be written as

$$\boldsymbol{\tau}_l = \mathbf{Y}_l(\mathbf{q}_l,\dot{\mathbf{q}}_l,\mathbf{e}_l,\dot{\mathbf{e}}_l)\hat{\boldsymbol{\theta}}_l + \mathbf{K}_l\boldsymbol{\epsilon}_l + \mathbf{B}\dot{\mathbf{e}}_l$$
$$\boldsymbol{\tau}_r = -\mathbf{Y}_r(\mathbf{q}_r,\dot{\mathbf{q}}_r,\mathbf{e}_r,\dot{\mathbf{e}}_r)\hat{\boldsymbol{\theta}}_r - \mathbf{K}_r\boldsymbol{\epsilon}_r - \mathbf{B}\dot{\mathbf{e}}_r.$$

The closed-loop system (1) and (3) is given by

$$\mathbf{M}_l(\mathbf{q}_l)\dot{\boldsymbol{\epsilon}}_l + \mathbf{C}_l(\mathbf{q}_l,\dot{\mathbf{q}}_l)\boldsymbol{\epsilon}_l + \mathbf{K}_l\boldsymbol{\epsilon}_l + \mathbf{B}\dot{\mathbf{e}}_l = \mathbf{Y}_l(\mathbf{q}_l,\dot{\mathbf{q}}_l,\mathbf{e}_l,\dot{\mathbf{e}}_l)\tilde{\boldsymbol{\theta}}_l + \boldsymbol{\tau}_h$$
$$\mathbf{M}_r(\mathbf{q}_r)\dot{\boldsymbol{\epsilon}}_r + \mathbf{C}_r(\mathbf{q}_r,\dot{\mathbf{q}}_r)\boldsymbol{\epsilon}_r + \mathbf{K}_r\boldsymbol{\epsilon}_r + \mathbf{B}\dot{\mathbf{e}}_r = \mathbf{Y}_l(\mathbf{q}_r,\dot{\mathbf{q}}_r,\mathbf{e}_r,\dot{\mathbf{e}}_r)\tilde{\boldsymbol{\theta}}_r - \boldsymbol{\tau}_e,$$

where $\tilde{\boldsymbol{\theta}}_i := \boldsymbol{\theta}_i - \hat{\boldsymbol{\theta}}_i$ is the error between the actual and the estimated physical parameters. The dynamics of the estimations of the uncertain parameters $\hat{\boldsymbol{\theta}}_i(t)$ are given by

$$\dot{\hat{\boldsymbol{\theta}}}_i = \boldsymbol{\Gamma}_i\mathbf{Y}_i^{\top}\boldsymbol{\epsilon}_i, \tag{5}$$

where $\boldsymbol{\Gamma}_i = \boldsymbol{\Gamma}_i^{\top}\in\mathbb{R}^{p\times p}$ are positive definite matrices.

The following proposition states the convergence claims of the previous result in [11].

Proposition 1. *Consider the bilateral teleoperator (1) in free motion ($\boldsymbol{\tau}_h = \boldsymbol{\tau}_e = \mathbf{0}$) controlled by Eq. (3) and using the parameter update law (5) together with Eq. (4). Then, for any constant time-delay T, all signals in the system are bounded. Moreover, position errors and velocities asymptotically converge to zero, i.e.,* $\lim_{t\to\infty}|\dot{\mathbf{q}}_i(t)| = \lim_{t\to\infty}|\mathbf{q}_l(t) - \mathbf{q}_r(t)| = 0$. □

The proof of the previous proposition exploited the cascade interconnection structure between the closed-loop teleoperator, (1) and (3), and the linear interconnection map (4). First, using the following Lyapunov–Krasovskiĭ candidate function

$$V = \frac{1}{2}\sum_{i\in\{l,r\}}\left[\boldsymbol{\epsilon}_i^{\top}\mathbf{M}_i\boldsymbol{\epsilon}_i + \tilde{\boldsymbol{\theta}}_i^{\top}\boldsymbol{\Gamma}_i^{-1}\tilde{\boldsymbol{\theta}}_i + \lambda\mathbf{e}_i^{\top}\mathbf{B}\mathbf{e}_i + \int_{t-T}^{t}\dot{\mathbf{q}}_i^{\top}\mathbf{B}\dot{\mathbf{q}}_i\,d\sigma\right],$$

it is shown that $\lim_{t\to\infty}|\boldsymbol{\epsilon}_i(t)| = \lim_{t\to\infty}|\dot{\mathbf{e}}_i(t)| = 0$. Then using the matrix representation of Eq. (4), together with a proper change of variables and its transformation to the frequency domain—using the Laplace transform—it is proved that $\lim_{t\to\infty}|\mathbf{e}_i(t)| = \lim_{t\to\infty}|\dot{\mathbf{q}}_i(t)| = 0$. The proof is concluded using the fact that since $\lim_{t\to\infty}\dot{\mathbf{q}}_i(t) = \mathbf{0}$ then $\lim_{t\to\infty}\int_{-T}^{0}\dot{\mathbf{q}}_i(t+\theta)\,d\theta = \mathbf{0}$.

3. The adaptive controller for the variable time-delays case

In this section the paper reports its main contribution, that is, the extension of controller (3) to the variable time-delays case. With regard to this extension, the following standard assumption is used.

A2. The variable time-delays have known upper bounds ${}^*T_i$, i.e., $0 \le T_i(t) \le {}^*T_i < \infty$. Additionally, the time-derivatives $\dot{T}_i(t)$ are bounded.

It should be noted that, contrary to [11], the time-delays can also be asymmetric. Since delays are now time-varying, the position errors in Eq. (2) change to[1]

$$\mathbf{e}_l := \mathbf{q}_l - \mathbf{q}_r(t - T_r(t)); \quad \mathbf{e}_r := \mathbf{q}_r - \mathbf{q}_l(t - T_l(t)), \tag{6}$$

and then

$$\begin{aligned} \dot{\mathbf{e}}_l &= \dot{\mathbf{q}}_l - (1 - \dot{T}_r(t))\dot{\mathbf{q}}_r(t - T_r(t)) \\ \dot{\mathbf{e}}_r &= \dot{\mathbf{q}}_r - (1 - \dot{T}_l(t))\dot{\mathbf{q}}_l(t - T_l(t)). \end{aligned} \tag{7}$$

The control objective in this paper is to asymptotically drive the local and the remote position errors (6) to zero in teleoperators with uncertain parameters and interconnecting variable time-delays. The local and the remote controllers are given by

$$\begin{aligned} \boldsymbol{\tau}_l &= \lambda \hat{\mathbf{M}}_l(\mathbf{q}_l)\dot{\mathbf{e}}_l + \lambda \hat{\mathbf{C}}_l(\mathbf{q}_l, \dot{\mathbf{q}}_l)\mathbf{e}_l - \hat{\mathbf{g}}_l(\mathbf{q}_l) + \mathbf{K}_l \boldsymbol{\epsilon}_l \\ \boldsymbol{\tau}_r &= -\lambda \hat{\mathbf{M}}_r(\mathbf{q}_r)\dot{\mathbf{e}}_r - \lambda \hat{\mathbf{C}}_r(\mathbf{q}_r, \dot{\mathbf{q}}_r)\mathbf{e}_r + \hat{\mathbf{g}}_r(\mathbf{q}_r) - \mathbf{K}_r \boldsymbol{\epsilon}_r. \end{aligned} \tag{8}$$

Compared to Eq. (3), these controllers do not contain the term $\mathbf{B}\dot{\mathbf{e}}_i$ and the position and velocity errors are calculated using Eqs. (6) and (7), respectively.

Invoking property P3, the teleoperator (1) in closed-loop with Eq. (8) is given by

$$\begin{aligned} \mathbf{M}_l(\mathbf{q}_l)\dot{\boldsymbol{\epsilon}}_l + \mathbf{C}_l(\mathbf{q}_l, \dot{\mathbf{q}}_l)\boldsymbol{\epsilon}_l + \mathbf{K}_l \boldsymbol{\epsilon}_l &= \mathbf{Y}_l(\mathbf{q}_l, \dot{\mathbf{q}}_l, \mathbf{e}_l, \dot{\mathbf{e}}_l)\tilde{\boldsymbol{\theta}}_l + \boldsymbol{\tau}_h \\ \mathbf{M}_r(\mathbf{q}_r)\dot{\boldsymbol{\epsilon}}_r + \mathbf{C}_r(\mathbf{q}_r, \dot{\mathbf{q}}_r)\boldsymbol{\epsilon}_r + \mathbf{K}_r \boldsymbol{\epsilon}_r &= \mathbf{Y}_r(\mathbf{q}_r, \dot{\mathbf{q}}_r, \mathbf{e}_r, \dot{\mathbf{e}}_r)\tilde{\boldsymbol{\theta}}_r - \boldsymbol{\tau}_e \end{aligned} \tag{9}$$

where $\boldsymbol{\epsilon}_i$ has been defined in Eq. (4). The controller gain $\mathbf{K}_i \in \mathbb{R}^{n \times n}$ is diagonal and positive definite.

Before going through the main result, let us present the following lemma, which has been borrowed from [8], that will be instrumental in the stability proofs.

Lemma 1. *For any vector signals* $\mathbf{x}, \mathbf{y} \in \mathbb{R}^n$, *any variable time-delay* $0 \le T(t) \le {}^*T < \infty$ *and any constant* $\alpha > 0$, *the following inequality holds*:

$$-\int_0^t \mathbf{x}^\top(\sigma) \int_{-T(\sigma)}^{0} \mathbf{y}(\sigma + \theta)\, d\theta\, d\sigma \le \frac{\alpha}{2}\|\mathbf{x}\|_2^2 + \frac{{}^*T^2}{2\alpha}\|\mathbf{y}\|_2^2.$$

3.1. Position error and velocity convergence to zero in free motion

In this section, it is considered that the human operator and the environment forces are zero. That is the same scenario as that analyzed in [11].

Proposition 2. *Consider the nonlinear teleoperator* (1) *in free motion* ($\boldsymbol{\tau}_h = \boldsymbol{\tau}_e = \mathbf{0}$) *and in closed-loop with the controller* (8) *and using the parameter estimation law* (5). *If the controller gain* λ *satisfies*

$$1 \ge \lambda({}^*T_l + {}^*T_r), \tag{10}$$

then, for any variable time-delay fulfilling assumption A2, *all signals in the system are bounded. Moreover, the local and remote position errors and velocities asymptotically converge to zero, i.e.,* $\lim_{t\to\infty}|\mathbf{q}_l(t) - \mathbf{q}_r(t)| = \lim_{t\to\infty}|\dot{\mathbf{q}}_i(t)| = 0$. □

[1] With some abuse of notation, the rest of the paper uses $\mathbf{e}_i$ for the position errors with variable delays.

Proof. Let us start by defining the following function:

$$W_i = \frac{1}{2}\boldsymbol{\epsilon}_i^\top \mathbf{M}_i(\mathbf{q}_i)\boldsymbol{\epsilon}_i + \frac{1}{2}\tilde{\boldsymbol{\theta}}_i^\top \boldsymbol{\Gamma}_i^{-1}\tilde{\boldsymbol{\theta}}_i. \tag{11}$$

From assumption A1, W_i is positive definite and radially unbounded with regard to $\boldsymbol{\epsilon}_i$ and $\tilde{\boldsymbol{\theta}}_i$. It can be easily verified, using property P1, that $\dot{W}_i$ along the closed-loop trajectories (9) is $\dot{W}_i = -\boldsymbol{\epsilon}_i^\top \mathbf{K}_i\boldsymbol{\epsilon}_i$.

Since $W_i \geq 0$, $\dot{W}_i \leq 0$ we conclude that $\boldsymbol{\epsilon}_i \in \mathcal{L}_2 \cap \mathcal{L}_\infty$ and $\tilde{\boldsymbol{\theta}}_i \in \mathcal{L}_\infty$. Now, consider

$$W = W_l + \frac{k_l}{k_r}W_r + \lambda k_l|\mathbf{q}_l - \mathbf{q}_r|^2, \tag{12}$$

where $k_i := \lambda_m\{\mathbf{K}_i\}$. Clearly, W is positive definite and radially unbounded with regard to $\boldsymbol{\epsilon}_i, \tilde{\boldsymbol{\theta}}_i$ and $|\mathbf{q}_l - \mathbf{q}_r|$. Its time-derivative is

$$\dot{W} = \dot{W}_l + \frac{k_l}{k_r}\dot{W}_r + 2\lambda k_l(\mathbf{q}_l - \mathbf{q}_r)^\top\left(\dot{\mathbf{q}}_l - \dot{\mathbf{q}}_r\right).$$

Using $\dot{W}_i \leq -k_i|\boldsymbol{\epsilon}_i|^2$ yields

$$\frac{1}{k_l}\dot{W} \leq -|\boldsymbol{\epsilon}_l|^2 - |\boldsymbol{\epsilon}_r|^2 + 2\lambda(\mathbf{q}_l - \mathbf{q}_r)^\top\left(\dot{\mathbf{q}}_l - \dot{\mathbf{q}}_r\right).$$

At this point, it is useful to express the errors (6) as

$$\mathbf{e}_l = \mathbf{q}_l - \mathbf{q}_r + \int_{t-T_r(t)}^{t}\dot{\mathbf{q}}_r(\sigma)\,d\sigma; \quad \mathbf{e}_r = \mathbf{q}_r - \mathbf{q}_l + \int_{t-T_l(t)}^{t}\dot{\mathbf{q}}_l(\sigma)\,d\sigma. \tag{13}$$

Now, using Eqs. (4) and (13) on $\dot{W}_i$, yields

$$\frac{1}{k_l}\dot{W} \leq -\lambda^2\left(|\mathbf{e}_l|^2 + |\mathbf{e}_r|^2\right) - |\dot{\mathbf{q}}_l|^2 - |\dot{\mathbf{q}}_r|^2 - 2\lambda\dot{\mathbf{q}}_l^\top\int_{t-T_r(t)}^{t}\dot{\mathbf{q}}_r(\sigma)\,d\sigma - 2\lambda\dot{\mathbf{q}}_r^\top\int_{t-T_l(t)}^{t}\dot{\mathbf{q}}_l(\sigma)\,d\sigma.$$

Note that W does not qualify as a Lyapunov Function, i.e., it does not satisfy $\dot{W} < 0$. Then, inspired by [22,8], let us integrate $\dot{W}$ from 0 to t. This returns

$$\frac{1}{k_l}W(t) - \frac{1}{k_l}W(0) \leq -\lambda^2\left(\|\mathbf{e}_l\|_2^2 + \|\mathbf{e}_r\|_2^2\right) - \|\dot{\mathbf{q}}_l\|_2^2 - \|\dot{\mathbf{q}}_r\|_2^2 - 2\lambda\int_0^t\dot{\mathbf{q}}_l^\top(\theta)\int_{\theta-T_r(\theta)}^{\theta}\dot{\mathbf{q}}_r(\sigma)\,d\sigma\,d\theta - 2\lambda\int_0^t\dot{\mathbf{q}}_r^\top(\theta)\int_{\theta-T_l(\theta)}^{\theta}\dot{\mathbf{q}}_l(\sigma)\,d\sigma\,d\theta.$$

Invoking Lemma 1 from [8] to the double integral terms, with α_l and α_r, respectively, yields

$$\frac{1}{k_l}W(t) - \frac{1}{k_l}W(0) \leq -\lambda^2\left(\|\mathbf{e}_l\|_2^2 + \|\mathbf{e}_r\|_2^2\right) - \psi_l\|\dot{\mathbf{q}}_l\|_2^2 - \psi_r\|\dot{\mathbf{q}}_r\|_2^2,$$

where

$$\psi_l := 1 - \lambda\alpha_l - \lambda\frac{{}^*T_l^2}{\alpha_r}, \quad \psi_r := 1 - \lambda\alpha_r - \lambda\frac{{}^*T_r^2}{\alpha_l}.$$

It is straightforward to show that there exist simultaneous solutions for $\psi_i > 0$ and for $\alpha_i > 0$ if λ fulfills $1 \geq \lambda({}^*T_l + {}^*T_r)$. If this inequality holds, there exists $\psi_i > 0$, such that

$$\frac{1}{k_l} W(t) + \lambda^2 \left(\|\mathbf{e}_l\|_2^2 + \|\mathbf{e}_r\|_2^2 \right) + \psi_l \|\dot{\mathbf{q}}_l\|_2^2 + \psi_r \|\dot{\mathbf{q}}_r\|_2^2 \leq \frac{1}{k_l} W(0).$$

Clearly $\mathbf{e}_i, \dot{\mathbf{q}}_i \in \mathcal{L}_2$ and $W \in \mathcal{L}_\infty$. This last and the fact that W is radially unbounded with respect to $|\mathbf{q}_l - \mathbf{q}_r|$ show that $|\mathbf{q}_l - \mathbf{q}_r| \in \mathcal{L}_\infty$. Further, using Eq. (6), $\dot{\mathbf{q}}_i \in \mathcal{L}_2$ and $|\mathbf{q}_l - \mathbf{q}_r| \in \mathcal{L}_\infty$ ensure that $\mathbf{e}_i \in \mathcal{L}_\infty$. Immediately, from Eq. (4) with $\boldsymbol{\epsilon}_i, \mathbf{e}_i \in \mathcal{L}_\infty$ it is also shown that $\dot{\mathbf{q}}_i \in \mathcal{L}_\infty$ which in turn—together with assumption A2—implies that $\dot{\mathbf{e}}_i \in \mathcal{L}_\infty$.

From the closed-loop system (9), assumption A1, properties P2 and P3, and all the previous bounded signals it is proved that $\dot{\boldsymbol{\epsilon}}_i \in \mathcal{L}_\infty$. This concludes the boundedness part of the proof.

Finally, the fact that $\dot{\boldsymbol{\epsilon}}_i, \dot{\mathbf{e}}_i \in \mathcal{L}_\infty$ and $\boldsymbol{\epsilon}_i, \mathbf{e}_i \in \mathcal{L}_2 \cap \mathcal{L}_\infty$ ensure, from Barbalăt's lemma, that

$$\lim_{t \to \infty} \boldsymbol{\epsilon}_i(t) = \lim_{t \to \infty} \mathbf{e}_i(t) = \mathbf{0}.$$

Since $\boldsymbol{\epsilon}_i = \dot{\mathbf{q}}_i + \lambda \mathbf{e}_i$ it is also concluded that $\lim_{t \to \infty} \dot{\mathbf{q}}_i(t) = \mathbf{0}$. Using Eq. (13) and the fact that since $\lim_{t \to \infty} \dot{\mathbf{q}}_i(t) = \mathbf{0}$ then $\lim_{t \to \infty} \int_{-T_i(\theta)}^{0} \dot{\mathbf{q}}_i(t + \theta)\, d\theta = \mathbf{0}$ concludes the proof. □

3.2. Stability properties when human and environment forces are not zero

Similar to [11], the previous proposition deals with the case when the human operator and the environment forces are zero. However, in general, these forces are not zero. In this scenario the following proposition outlines some stability results when these forces are not zero but they belong to a certain set of functions. It should be underscored that most of the previous works [3,4,23] rely on the assumption that the human operator/environment can be modeled as velocity to force (strictly) passive maps. An insightful exception to these cases are the works of [24,25], where the human operator/environment can exhibit non-passive behaviors.

Proposition 3. *Consider the nonlinear teleoperator (1) in closed-loop with the controller (8) and using the parameter estimation law (5). Then*

(i) *if the human operator and environment forces are bounded, i.e.,* $\boldsymbol{\tau}_h, \boldsymbol{\tau}_e \in \mathcal{L}_\infty$, *then* $\boldsymbol{\epsilon}_i \in \mathcal{L}_\infty$,
(ii) *if* $\boldsymbol{\tau}_h, \boldsymbol{\tau}_e \in \mathcal{L}_2$ *and assumption* A2 *and condition (10) hold, then all signals are bounded and* $\mathbf{e}_i, \dot{\mathbf{q}}_i \in \mathcal{L}_2$,
(iii) *if* $\boldsymbol{\tau}_h, \boldsymbol{\tau}_e \in \mathcal{L}_\infty \cap \mathcal{L}_2$ *and assumption* A2 *and condition (10) hold, then all signals are bounded and*

$$\lim_{t \to \infty} |\mathbf{q}_l(t) - \mathbf{q}_r(t)| = \lim_{t \to \infty} |\dot{\mathbf{q}}_i(t)| = 0. \qquad \square$$

Proof. Claim (i) is established using Eq. (11). In this case, $\dot{W}_i = -\boldsymbol{\epsilon}_i^\top \mathbf{K}_i \boldsymbol{\epsilon}_i + \boldsymbol{\epsilon}_i^\top \mathbf{u}_i$, where $u_i := \{\boldsymbol{\tau}_h, -\boldsymbol{\tau}_e\}$. Using Young's inequality yields $\dot{W}_i \leq -(k_i/2)|\boldsymbol{\epsilon}_i|^2 + (1/2k_i)|\mathbf{u}_i|^2$, where $k_i := \lambda_m\{\mathbf{K}_i\}$. Since $\mathbf{u}_i \in \mathcal{L}_\infty$, clearly, if $|\boldsymbol{\epsilon}_i|^2 > (1/k_i^2)|\mathbf{u}_i|^2$ then there exists $\beta_i \in \mathbb{R}_{>0}$ such that $\dot{W}_i \leq -\beta_i |\boldsymbol{\epsilon}_i|^2$. This last and the fact that W_i is positive definite and radially unbounded with regard to $\boldsymbol{\epsilon}_i$ ensure that $\boldsymbol{\epsilon}_i \in \mathcal{L}_\infty$.

The proof of Claim (ii) employs the Lyapunov–Razumikhin functional (12). Proceeding *verbatim* as in the proof of Proposition 2, if assumption A2 and condition (10) hold, it is shown

that

$$\frac{1}{k_l}W(0)+\delta_l\|\boldsymbol{\tau}_h\|_2^2+\delta_r\|\boldsymbol{\tau}_e\|_2^2\geq\frac{\lambda^2}{2}\left(\|\mathbf{e}_l\|_2^2+\|\mathbf{e}_r\|_2^2\right)+\frac{\psi_l}{2}\|\dot{\mathbf{q}}_l\|_2^2+\frac{\psi_r}{2}\|\dot{\mathbf{q}}_r\|_2^2+\frac{1}{k_l}W(t),$$

where we applied Young's inequality in the crossed terms $\boldsymbol{\epsilon}_l^\top\boldsymbol{\tau}_h$ and $\boldsymbol{\epsilon}_r^\top\boldsymbol{\tau}_e$ before integration and $\delta_l:=1/2\lambda^2+1/2\psi_l$ and $\delta_r:=1/2\lambda^2+1/2\psi_r$.

Since, in this case, $\boldsymbol{\tau}_h,\boldsymbol{\tau}_e\in\mathcal{L}_2$ then $\mathbf{e}_i,\dot{\mathbf{q}}_i\in\mathcal{L}_2$. Moreover, the fact that $W\geq 0$ ensures that $W\in\mathcal{L}_\infty$ and hence $\boldsymbol{\epsilon}_i,\tilde{\boldsymbol{\theta}}_i,|\mathbf{q}_l-\mathbf{q}_r|\in\mathcal{L}_\infty$. Further, with $|\mathbf{q}_l-\mathbf{q}_r|\in\mathcal{L}_\infty$ and $\dot{\mathbf{q}}_i\in\mathcal{L}_2$ it can be established that $\mathbf{e}_i\in\mathcal{L}_\infty$. This last and the fact that $\boldsymbol{\epsilon}_i$ is bounded prove that $\dot{\mathbf{q}}_i\in\mathcal{L}_\infty$. This completes the proof of part (ii).

The proof of Claim (iii) follows *verbatim* the last part of the proof of Proposition 2 with the additional fact that $\boldsymbol{\tau}_h,\boldsymbol{\tau}_e\in\mathcal{L}_\infty\cap\mathcal{L}_2$ from which it can be established, from the closed-loop system (9), that $\dot{\boldsymbol{\epsilon}}_i\in\mathcal{L}_\infty$. The proof is completed using Barbalăt's Lemma. □

3.3. Additional remarks

Remark 1. The proposed stability analysis for the *variable* time-delays case is based on simple Lyapunov-like functions and thus is more straightforward than the one appearing in [11]. In such work, apart from the fact that it considers only *constant* time-delays, the stability analysis is cumbersome and involves the use of Lyapunov–Krasovskiĭfunctionals and frequency domain techniques.

Remark 2. Compared to [11], no additional damping terms, like $-\mathbf{B}\dot{\mathbf{e}}_i$, need to be incorporated to prove the convergence of position errors and velocities to zero.

Remark 3. In order to compute $\dot{T}_i(t)$ at both ends, the value of a new function $f_i(t)$ is sent through the communications together with position and velocity data. Thus, when $f_i(t)$ arrives at its destination it has the value $f_i(t-T_i(t))$. Hence, $\dot{T}_i(t)$ can be estimated, indirectly, from $\dot{f}_i(t-T_i(t))=\dot{f}_i(t)[1-\dot{T}_i(t)]$. Designing $f_i(t)$ s.t. $\dot{f}_i(t)=1$ yields $\dot{T}_i(t)=1-\dot{f}_i(t-T_i(t))$. Hence, $\dot{T}_i(t)$ can be obtained without knowledge of $T_i(t)$.

4. Simulations

To show the effectiveness of the proposed scheme, some simulations are presented. In these simulations the local and remote manipulators are modeled as a pair of 2 DOF serial links with revolute joints (cf. Fig. 1). Their corresponding nonlinear dynamics are modeled by Eq. (1). In what follows $\alpha_i:=l_{2_i}^2m_{2_i}+l_{1_i}^2(m_{1_i}+m_{2_i})$, $\beta_i:=l_{1_i}l_{2_i}m_{2_i}$ and $\delta_i:=l_{2_i}^2m_{2_i}$. The inertia matrices $\mathbf{M}_i(\mathbf{q}_i)$ are given by

$$\mathbf{M}_i(\mathbf{q}_i)=\begin{bmatrix}\alpha_i+2\beta_i\mathrm{c}_{2_i} & \delta_i+\beta_i\mathrm{c}_{2_i}\\ \delta_i+\beta_i\mathrm{c}_{2_i} & \delta_i\end{bmatrix}.$$

c_{2_i} is the short notation for $\cos(q_{2_i})$. q_{k_i} is the articular position of link k of manipulator i, with $k\in\{1,2\}$. The Coriolis and centrifugal effects are modeled by

$$\mathbf{C}_i(\mathbf{q}_i,\dot{\mathbf{q}}_i)=\begin{bmatrix}-\beta_i\mathrm{s}_{2_i}\dot{q}_{2_i} & -\beta_i\mathrm{s}_{2_i}(\dot{q}_{1_i}+\dot{q}_{2_i})\\ \beta_i\mathrm{s}_{2_i}\dot{q}_{1_i} & 0\end{bmatrix}.$$

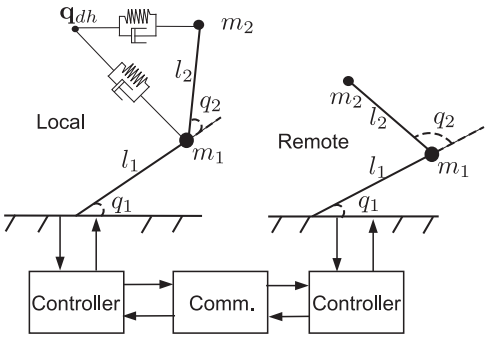

Fig. 1. Simulations scheme.

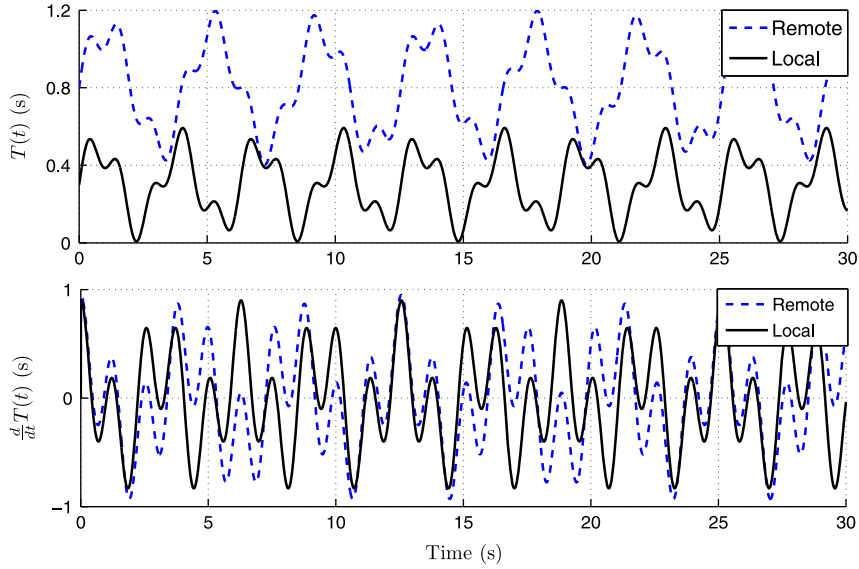

Fig. 2. Variable time-delay employed in the simulations.

s_{2_i} is the short notation for $\sin(q_{2_i})$. $\dot{q}_{1_i}$ and $\dot{q}_{2_i}$ are the respective revolute velocities of the two links. The gravity forces $\mathbf{g}_i(\mathbf{q}_i)$ for each manipulator are represented by

$$\mathbf{g}_i(\mathbf{q}_i) = \begin{bmatrix} \frac{1}{l_{2_i}} g\delta_i c_{12_i} + \frac{1}{l_{1_i}}(\alpha_i - \delta_i)c_{1_i} \\ \frac{1}{l_{2_i}} g\delta_i c_{12_i} \end{bmatrix},$$

c_{12_i} stands for $\cos(q_{1_i} + q_{2_i})$. l_{k_i} and m_{k_i} are the respective lengths and masses of each link.

The following parametrization $\mathbf{Y}(\mathbf{q}, \dot{\mathbf{q}}, \mathbf{e}, \dot{\mathbf{e}})$ is proposed for both manipulators:

$$\mathbf{Y} = \begin{bmatrix} \lambda\dot{e}_1 & \lambda Y_{12} & \lambda\dot{e}_2 & -g c_{12} & -g c_1 \\ 0 & \lambda(c_2\dot{e}_1 + s_2\dot{q}_1 e_1) & \lambda(\dot{e}_1 + \dot{e}_2) & g c_{12} & 0 \end{bmatrix},$$

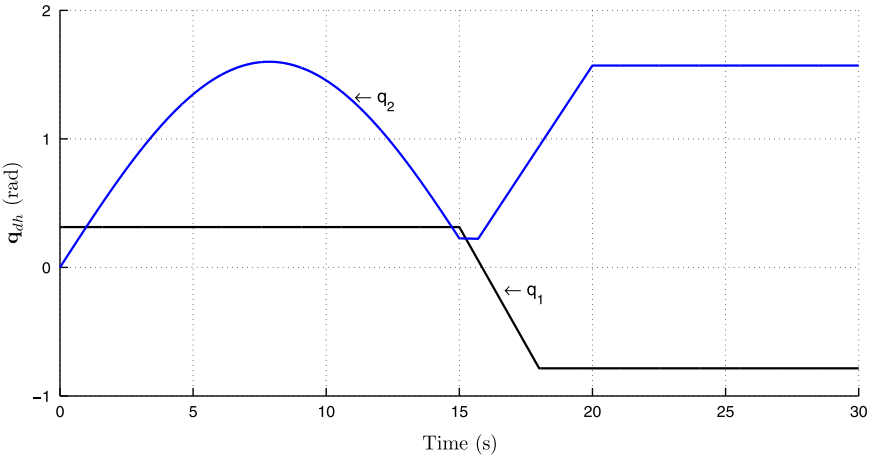

Fig. 3. Desired human position.

$$\boldsymbol{\theta} = \left[\alpha \;\; \beta \;\; \delta \;\; \frac{1}{l_2}\delta \;\; \frac{1}{l_1}(\alpha-\delta)\right]^{\top},$$

where $Y_{12} = 2c_2\dot{e}_1 + c_2\dot{e}_2 - s_2(\dot{q}_{1_i} + \dot{q}_{2_i})e_2 - s_2\dot{q}_2 e_1$.

The physical parameters for the manipulators are the length of links l_{1_i} and l_{2_i} is 0.38 m, for both manipulators; the masses for the links are $m_{1_l} = 1.5$ kg, $m_{2_l} = 0.75$ kg, $m_{1_r} = 2.5$ kg and $m_{2_r} = 1.5$ kg.

The initial conditions are $\dot{\mathbf{q}}_i(0) = \mathbf{0}$ and $\mathbf{q}_l^{\top}(0) = [-1/8\pi; 1/8\pi]$, $\mathbf{q}_r^{\top}(0) = [1/6\pi; -1/4\pi]$.

The time-delays have been set as $T_l(t) = 0.3 + 0.2\,\sin(2t) + 0.1\,\sin(5t)$ and $T_r(t) = 0.8 + 0.3\,\sin(1.5t) + 0.1\,\sin(5t)$. The bounds of the delays are ${}^{*}T_l = 0.6$ and ${}^{*}T_r = 1.2$. These variable time-delays and their derivatives can be seen in Fig. 2.

The controller gains are set as $\mathbf{K}_l = 5\mathbf{I}_2$, $\mathbf{K}_r = 15\mathbf{I}_2$ and $\boldsymbol{\Gamma}_l = \boldsymbol{\Gamma}_r = 0.5\mathbf{I}_5$. Further, λ is set fulfilling Eq. (10) as $\lambda = 0.5$.

The human operator is modeled as the spring–damper system $\boldsymbol{\tau} = K_h(\mathbf{q}_d - \mathbf{q}_l) - d\dot{\mathbf{q}}_l$ where $K_h = 25$ and $d = 5$. Fig. 3 depicts the desired human position $\mathbf{q}_{dh}$.

4.1. Remote manipulator in free space

In this section, the simulations in which the remote manipulator moves without contact with its environment are presented. In this case, from Fig. A2, it can be observed that position tracking between the local and the remote manipulators is established. Moreover, Fig. A3 shows that local and remote velocities asymptotically converge to zero. Finally, Figs. A4 and A5 depict the time evolution of the torques of the local and the remote controllers and the estimated parameters respectively, which are clearly bounded.

4.2. Remote manipulator interacting with a rigid wall

In this set of simulations, a rigid wall is added in the remote environment. The wall is located in the xz-plane at $y = 0.3$ m. It is modeled as a spring–damper Cartesian system with stiffness equal to 20 000 N m and damping equal to 200 N m/s.

For this case, Figs. A6 and A7 show the position tracking capabilities of the proposed controller in Cartesian space and in joint space, respectively. From these figures it is concluded that, despite variable time-delays and a rigid interaction with the environment, position error converges to zero and hence position tracking is established. Fig. A8 presents the local and remote velocities, Fig. A9 shows the exerted torques of the local and the remote controllers and Fig. A10 depicts the evolution of the estimated parameters.

5. Experiments

The experimental setup is composed of two fully actuated 3-DOF, PHANToM Omni® devices, from Sensable Technologies (http://sensable.com/). These devices run in the same computer in Matlab Simulink® (see Fig. 4). For handling the computer-device communication, the PHANSIM Libraries [26] have been used. The induced time-delays between the local and the remote manipulators are the same as those used in the simulations, and are depicted in Fig. 2.

The PHANToM Omni dynamical parametrization, in property P3, has been borrowed from [27]. Such parametrization is given by the pair $\mathbf{Y}(\mathbf{q},\dot{\mathbf{q}},\mathbf{x},\mathbf{y})\in\mathbb{R}^{3\times 8}$ and $\boldsymbol{\theta}\in\mathbb{R}^8$, where $\mathbf{x},\mathbf{y}\in\mathbb{R}^3$. The elements of matrix $\mathbf{Y}$ are for the first raw, $Y_{11}=y_1c_{22}-x_2s_{22}\dot{q}_1-x_1s_{22}\dot{q}_2$, $Y_{12}=y_1c_{22,23}\ -s_{22,23}\dot{q}_1(x_2+x_3)-x_1s_{22,23}(\dot{q}_2-\dot{q}_3)$, $Y_{13}=y_1\left(s_{22,3}+s_3\right)+\frac{1}{2}c_3\left(x_1\dot{q}_3+x_3\dot{q}_1\right)+c_{22,3}\left(x_2\dot{q}_1+\frac{1}{2}x_3\dot{q}_1+x_1\dot{q}_2+\frac{1}{2}x_1\dot{q}_3\right)$, $Y_{14}=y_1$ and $Y_{15}=Y_{16}=Y_{17}=Y_{18}=0$; for the second raw, $Y_{21}=x_1s_{22}\dot{q}_1$, $Y_{22}=x_1s_{22,23}\dot{q}_1$, $Y_{23}=c_3x_3(\dot{q}_2+\dot{q}_3)+\ x_2c_3\dot{q}_3-x_1c_{22,3}\dot{q}_1+2y_2s_3+y_3s_3$, $Y_{24}=0$, $Y_{25}=y_2$, $Y_{26}=y_3$, $Y_{27}=s_{2,3}$ and $Y_{28}=c_2$; and for the third raw, $Y_{31}=Y_{34}=Y_{35}=Y_{38}=0$, $Y_{32}=x_1s_{22,23}\dot{q}_1$, $Y_{33}=y_2s_3-\frac{1}{2}\dot{q}_1\ \ x_1\left(c_{22,3}+c_3\right)-x_2c_3\dot{q}_2$, $Y_{36}=y_2+y_3$ and $Y_{37}=s_{2,3}$.

To shorten the previous equations, the following notation has been defined. For any joint positions q_j, q_k, $j,k\in[1,3]$, $s_j,c_j,s_{jk},c_{jk},s_{2j},c_{2j},s_{2j,k},c_{2j,k},s_{2j,2k}$ and $c_{2j,2k}$ are the short notation of $\sin(q_j)$, $\cos(q_j)$, $\sin(q_j+q_k)$, $\cos(q_j+q_k)$, $\sin(2q_j)$, $\cos(2q_j)$, $\sin(2q_j+q_k)$, $\cos(2q_j+q_k)$, $\sin(2q_j+2q_k)$ and $\cos(2q_j+2q_k)$, respectively.

The elements of the physical parameter vectors are $\theta_1=m_3\ell_1^2+\frac{1}{4}m_2\ell_1^2+I_{2x}-I_{2y}$, $\theta_2=-\frac{1}{4}m_3\ell_2^2-I_{3y}+I_{3z}$, $\theta_3=m_3\ell_1\ell_2$, $\theta_4=\frac{1}{4}m_2\ell_1^2+\frac{1}{4}m_3\ell_2^2+m_3\ell_1^2+I_{2z}+I_{3y}+I_{2y}+I_{3z}+2I_{1x}$, $\theta_5=\frac{1}{2}m_3\ell_2^2+2m_3\ell_1^2+\frac{1}{2}m_2\ell_1^2+2I_{2x}+2I_{3x}$, $\theta_6=\frac{1}{2}m_3\ell_2^2+2I_{3x}$, $\theta_7=m_3g\ell_2$ and

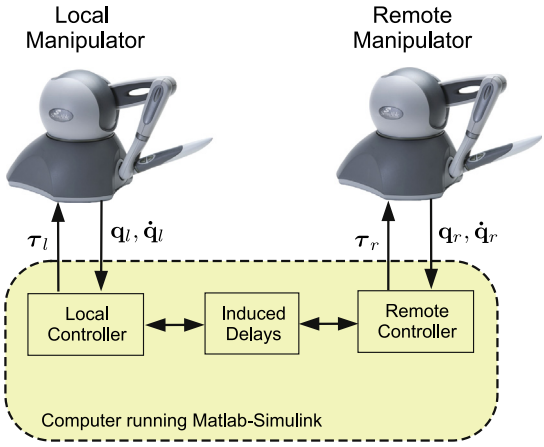

Fig. 4. Experimental setup, composed of two PHANToM Omni® devices.

$\theta_8 = m_3 g \ell_1 + m_2 g \ell_1$, where m_j is the mass of link j, ℓ_j is the j-link length, I_{jk} is the moment of inertia of link j along the direction k and g is the gravity constant.

Controllers (8) have been implemented using the previous parametrization with $\mathbf{x}_i = -\lambda \mathbf{e}_i$ and $\mathbf{y}_i = -\lambda \dot{\mathbf{e}}_i$ with the following control gains $\mathbf{K}_i = 0.5\mathbf{I}_3$, $\mathbf{\Gamma}_i = 0.02\mathbf{I}_8$ and $\lambda = 0.7$.

Similar to the simulations, the experiments are performed in two different scenarios: (a) when the remote manipulator is in free space and (b) when it interacts with a stiff object.

5.1. Remote manipulator in free space

Fig. A11 and A12 depict the joint position and velocity, respectively, of the local and remote manipulators for the case when the remote robot moves freely in the space. In this case, the human operator injects forces to the local manipulator and the remote manipulator follows its position. It can be concluded that both, position error and velocity, asymptotically converge to zero, as expected.

5.2. Remote manipulator interacting with a rigid object

Figs. A13–A15 depict the experimental results for the case when the remote manipulator interacts with a stiff object (wooden box). The local and remote Cartesian positions and joint positions are shown in Fig. A13 and in Fig. A14, respectively. Note that the remote manipulator comes in contact with the stiff object from around 5 s to 13 s. Even in the presence of variable time-delays and stiff contacts, the position error and the velocities (Fig. A15) asymptotically converge to zero.

6. Conclusions and future work

This work proposes an adaptive controller for general nonlinear teleoperators with *variable* time-delays. The adaptive controller can be seen as a significant extension of the previous schemes reported in [11]. The proposed controller excels the previous one in two main aspects: the time-delays can be asymmetric and variable and it injects less damping, since the new controller does not contain the term $\mathbf{B}_i \dot{\mathbf{e}}_i$. The scheme reported here provides a sufficient condition under which, in free motion, all signals in the system are bounded and position errors and velocities asymptotically converge to zero. Moreover, it also outlines some input–output stability properties when the human operator and environment forces are not zero but bounded.

Simulations and experiments with two nonlinear manipulators evidence the performance of the proposed approach.

Future work includes the extension of this framework to the more general case of synchronization of networks of Euler–Lagrange systems with variable time-delays in the interconnection.

It should be underscored that, in order to apply the proposed controller (8), the regressor matrices $\mathbf{Y}_i$ have to be known. For high DOF manipulators, the computation of such regressor might be a daunting task. In order to overcome this issue, another future research avenue is to employ a neural network controller [28–32], a fuzzy logic controller [33] or the combination of both schemes [34], to approximate the nonlinear behavior of the nonlinear teleoperator.

Appendix A. Simulations and experiments figures

This appendix presents, graphically, the simulations and the experiments results in Figs. A1-A15 below.

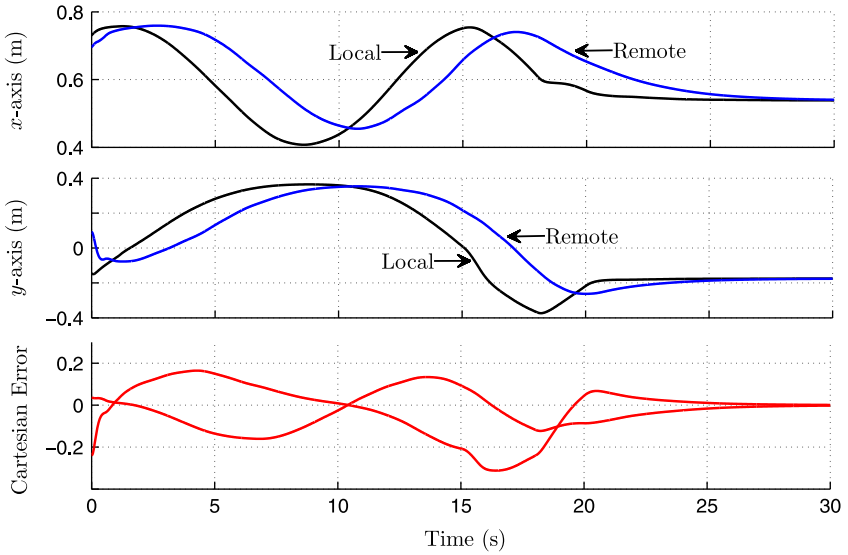

Fig. A1. Simulation results for the Cartesian position when the remote manipulator moves in free space.

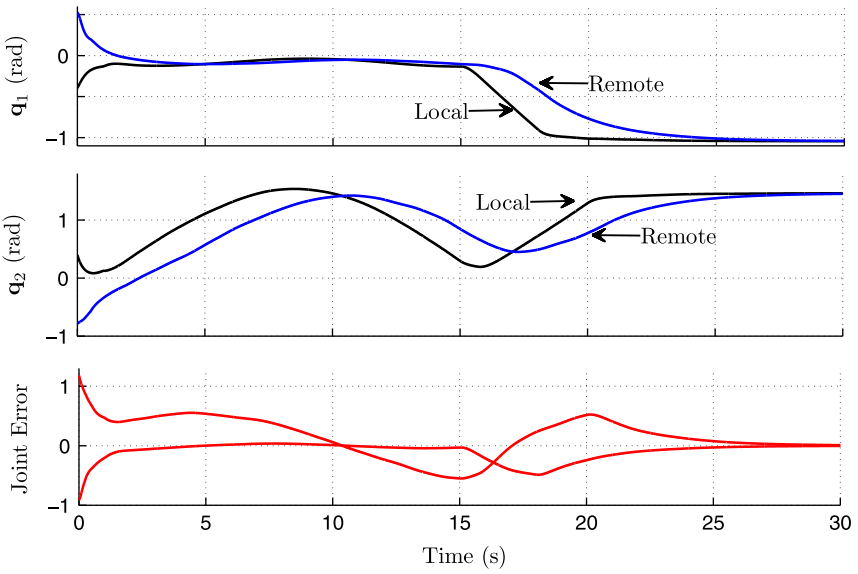

Fig. A2. Simulation results for joint position and error when the remote manipulator moves in free space.

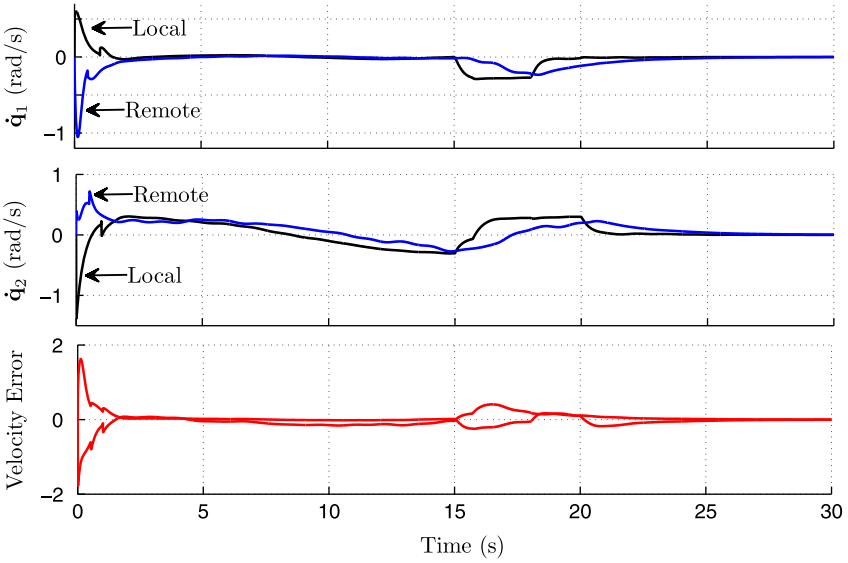

Fig. A3. Simulation results for joint velocities in free space.

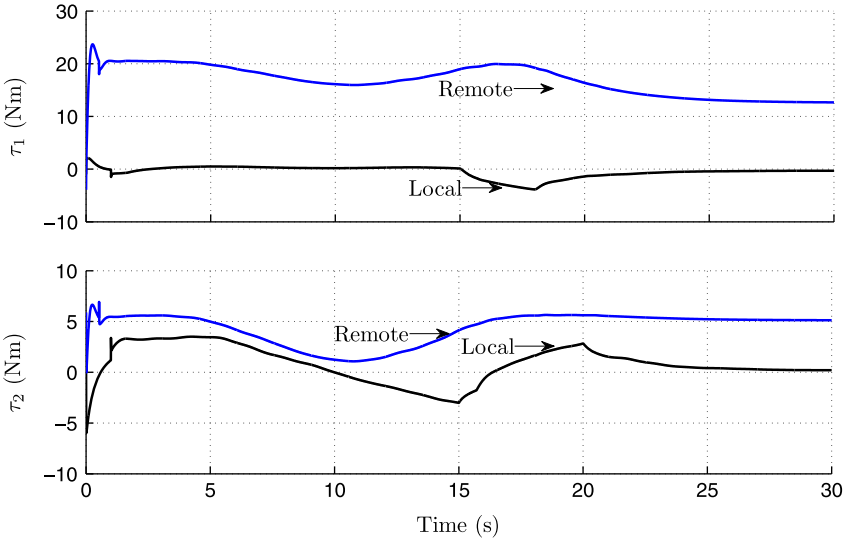

Fig. A4. Simulation results for the torques of the local and the remote controllers in free space.

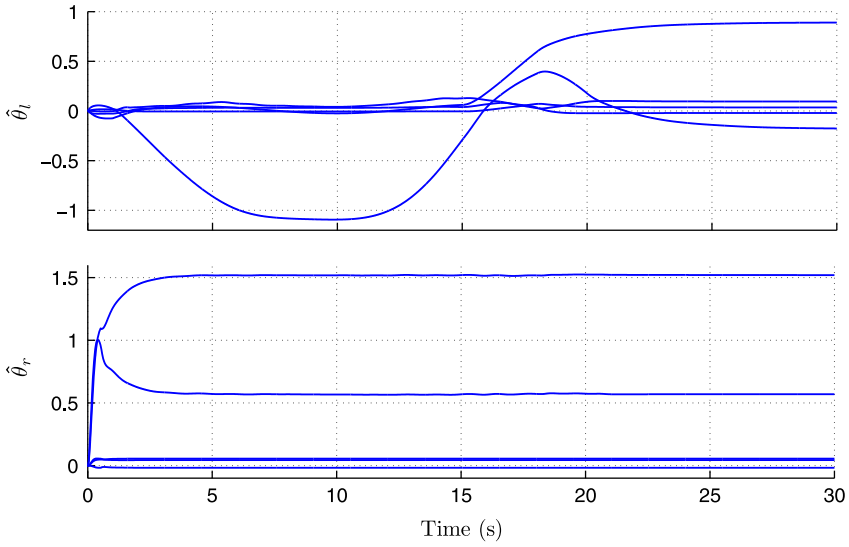

Fig. A5. Simulation results for the estimated parameters $\hat{\boldsymbol{\theta}}_i(t)$ in free space.

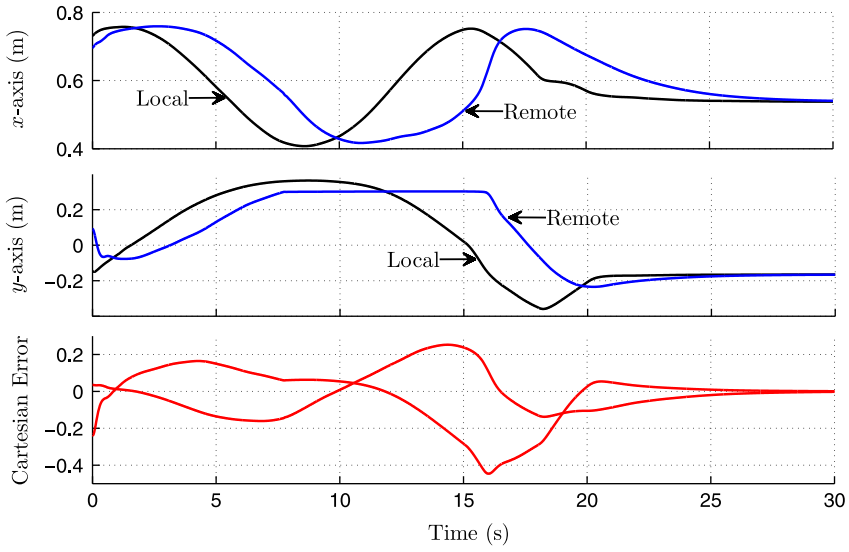

Fig. A6. Simulation results for the Cartesian position when the remote manipulator interacts with a rigid wall, located at $y_r = 0.3$ m.

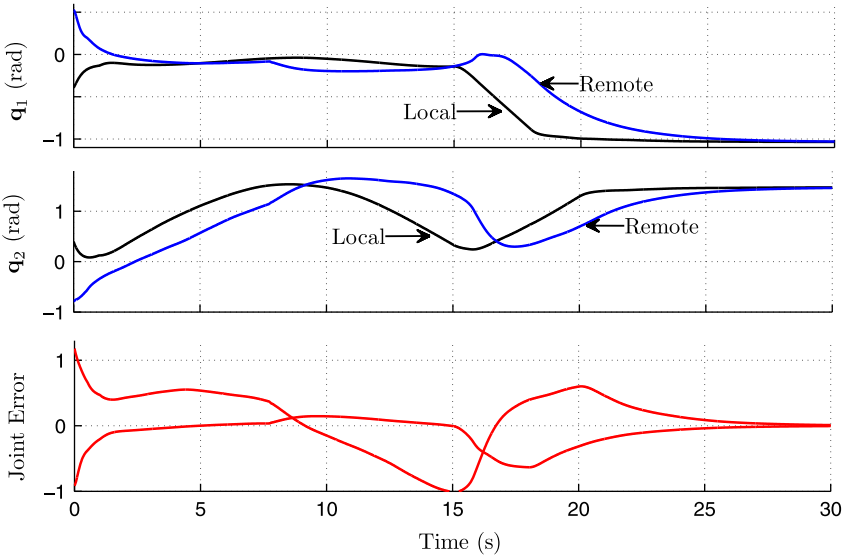

Fig. A7. Simulation results for joint position and error when interacting with a remote rigid wall.

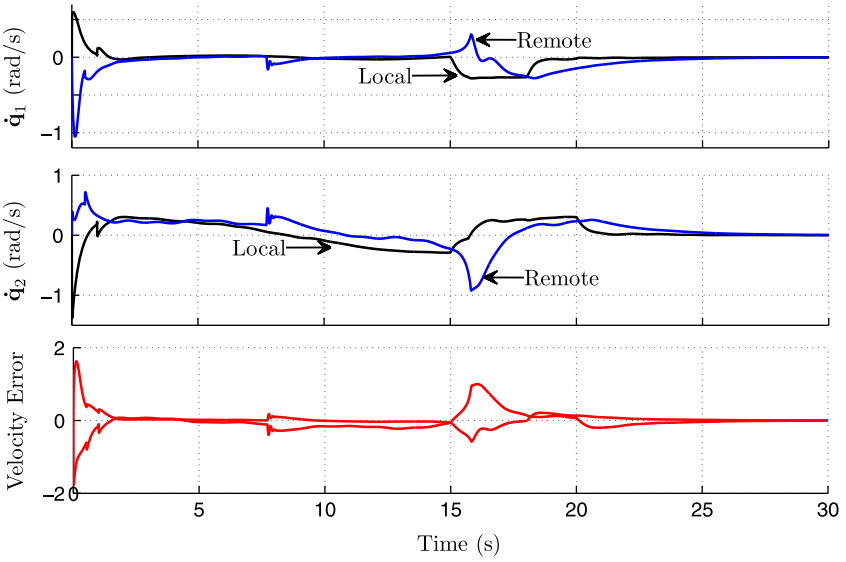

Fig. A8. Simulation results for joint velocities when interacting with a remote rigid wall.

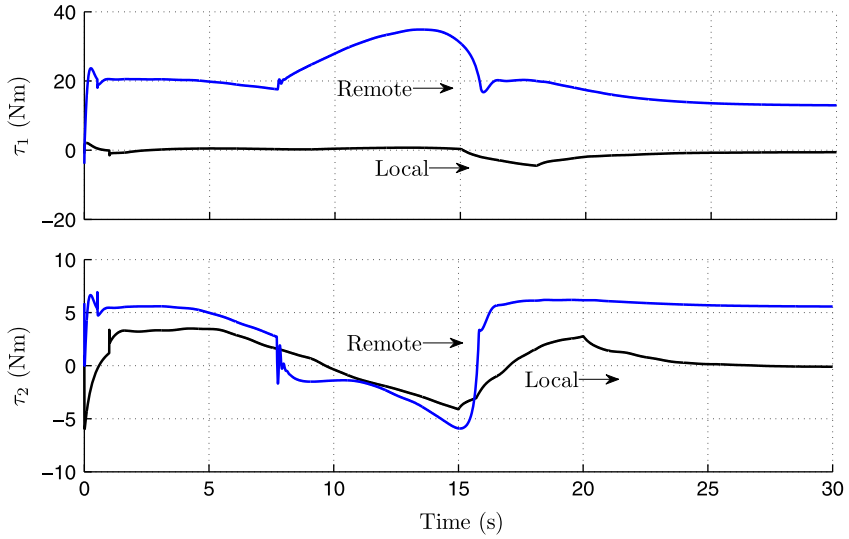

Fig. A9. Simulation results for the torques of the local and the remote controllers when interacting with a remote rigid wall.

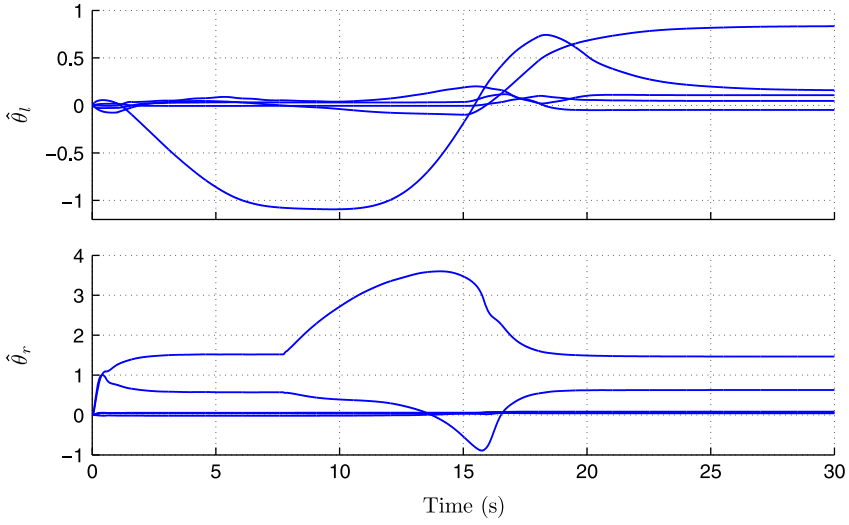

Fig. A10. Simulation results for the estimated parameters $\hat{\boldsymbol{\theta}}_i(t)$ when interacting with a remote rigid wall.

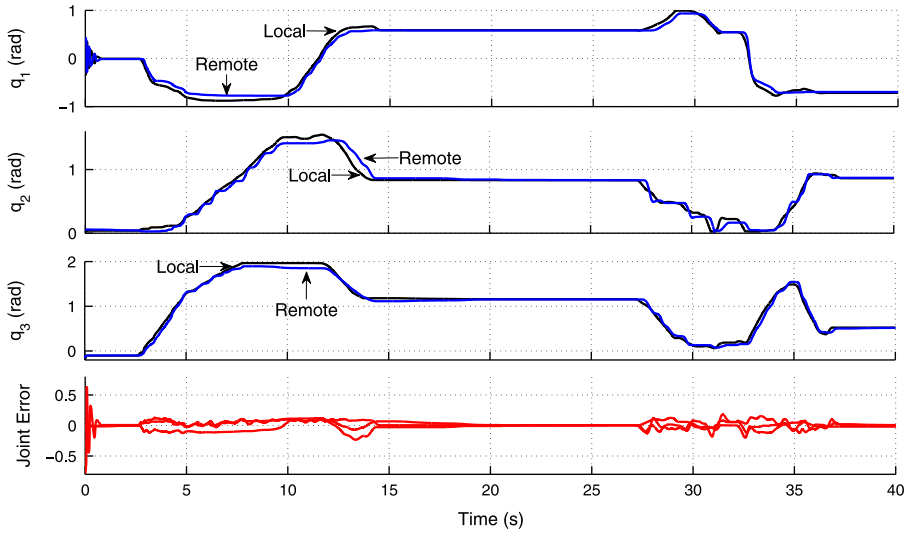

Fig. A11. Joint positions of the local and the remote PHANToM Omni when the remote manipulator moves in free space.

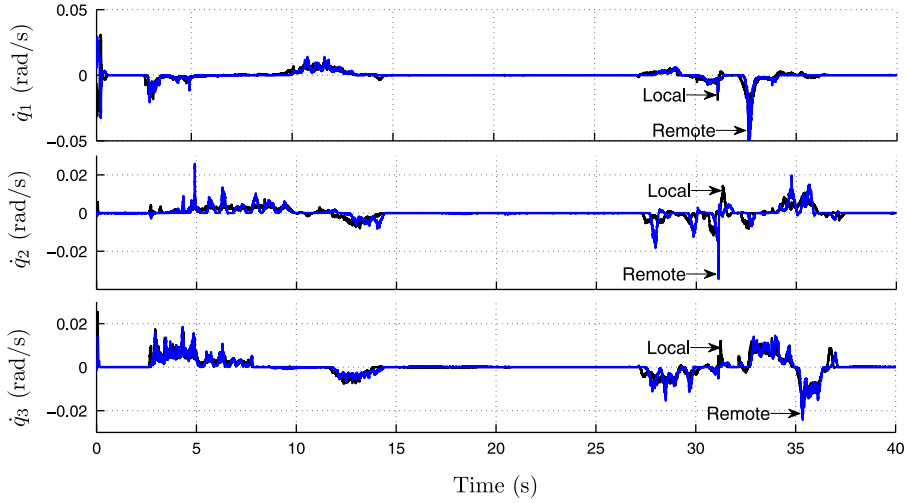

Fig. A12. Joint velocities of the local and the remote PHANToM Omni when the remote manipulator moves in free space.

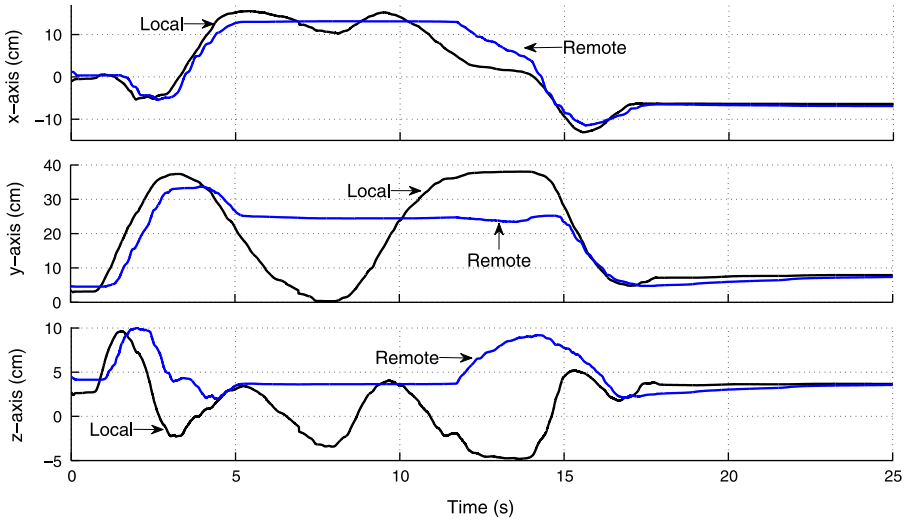

Fig. A13. Experimental results for the Cartesian position of the local and remote manipulators when the remote interacts with a stiff object.

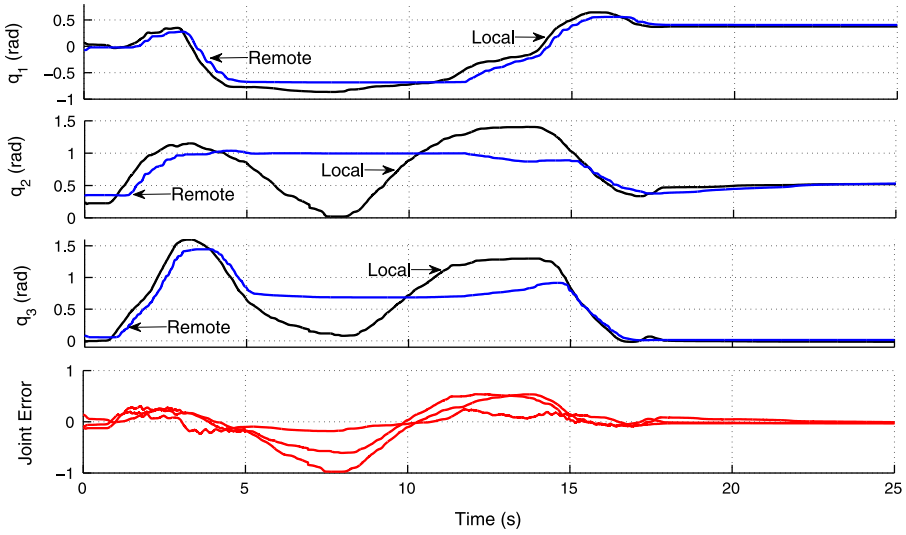

Fig. A14. Experimental results for the joint positions of the local and remote manipulators when the remote interacts with a stiff object.

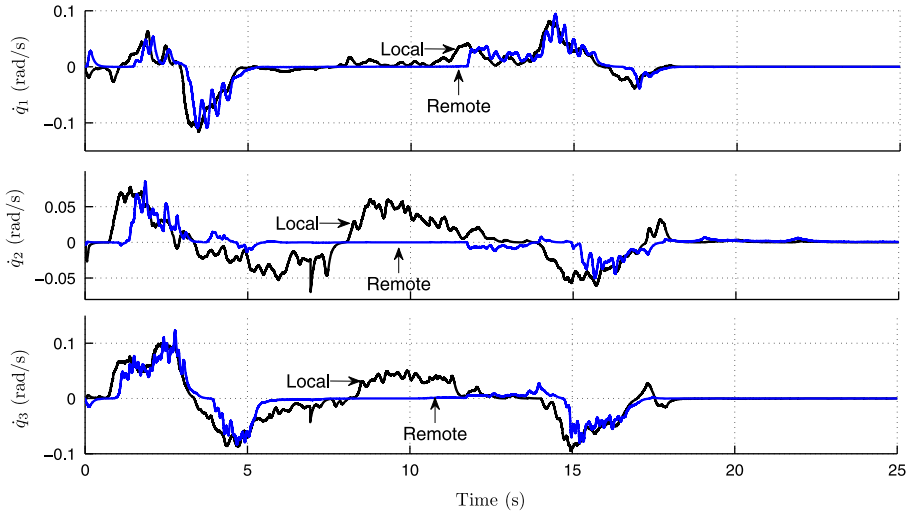

Fig. A15. Behavior of the local and remote PHANToM Omni joint velocities when the remote Omni interacts with a stiff object.

References

[1] R.J. Anderson, M.W. Spong, Bilateral control of teleoperators with time delay, IEEE Trans. Autom. Control 34 (May (5)) (1989) 494–501.
[2] G. Niemeyer, J.J. Slotine, Stable adaptive teleoperation, IEEE J. Ocean. Eng. 16 (January (1)) (1991) 152–162.
[3] P.F. Hokayem, M.W. Spong, Bilateral teleoperation: an historical survey, Automatica 42 (12) (2006) 2035–2057.
[4] E. Nuño, L. Basañez, R. Ortega, Passivity-based control for bilateral teleoperation: a tutorial, Automatica 47 (March (3)) (2011) 485–495.
[5] N. Chopra, M.W. Spong, R. Ortega, N. Barbanov, On tracking performance in bilateral teleoperation, IEEE Trans. Robot. 22 (August (4)) (2006) 844–847.
[6] D. Lee, M.W. Spong, Passive bilateral teleoperation with constant time delay, IEEE Trans. Robot. 22 (April (2)) (2006) 269–281.
[7] E. Nuño, R. Ortega, N. Barabanov, L. Basañez, A globally stable PD controller for bilateral teleoperators, IEEE Trans. Robot. 24 (June (3)) (2008) 753–758.
[8] E. Nuño, L. Basañez, R. Ortega, M.W. Spong, Position tracking for nonlinear teleoperators with variable time-delay, Int. J. Robot. Res. 28 (7) (2009) 895–910.
[9] N. Chopra, M.W. Spong, Output synchronization of nonlinear systems with time delay in communication, in: Proceedings of the IEEE Conference on Decision and Control, December 2006, pp. 4986–4992.
[10] N. Chopra, M.W. Spong, R. Lozano, Synchronization of bilateral teleoperators with time delay, Automatica 44 (August (8)) (2008) 2142–2148.
[11] E. Nuño, R. Ortega, L. Basañez, An adaptive controller for nonlinear bilateral teleoperators, Automatica 46 (January (1)) (2010) 155–159.
[12] E. Nuño, R. Ortega, L. Basañez, D. Hill, Synchronization of networks of nonidentical Euler–Lagrange systems with uncertain parameters and communication delays, IEEE Trans. Autom. Control 56 (April (4)) (2011) 935–941.
[13] F. Hashemzadeh, I. Hassanzadeh, M. Tavakoli, G. Alizadeh, Adaptive control for state synchronization of nonlinear haptic telerobotic systems with asymmetric varying time delays, J. Intell. Robot. Syst. 68 (3-4) (2012) 245–259.
[14] N. Chopra, P. Berestesky, M.W. Spong, Bilateral teleoperation over unreliable communication networks, IEEE Trans. Control Syst. Technol. 16 (2) (2008) 304–313.
[15] J.H. Ryu, J. Artigas, C. Preusche, A passive bilateral control scheme for a teleoperator with time-varying communication delay, Mechatronics 20 (7) (2010) 812–823.
[16] C. Secchi, S. Stramigioli, C. Fantuzzi, Variable delay in scaled port-Hamiltonian telemanipulation, Mechatronics 18 (7) (2008) 357–363.

[17] E. Nuño, R. Ortega, L. Basañez, Erratum to "an adaptive controller for nonlinear teleoperators" [Automatica 46 (2010) 155–159], Automatica 47 (May (5)) (2011) 1093–1094.
[18] E. Nuño, I. Sarras, L. Basañez, An adaptive controller for nonlinear teleoperators: the variable time-delays case, in: IFAC World Congress, Cape Town, South Africa, 2014.
[19] R. Ortega, A. Loria, P.J. Nicklasson, H.J. Sira-Ramirez, Passivity-based Control of Euler–Lagrange Systems: Mechanical, Electrical and Electromechanical Applications, Springer, New York, USA, 1998.
[20] R. Kelly, V. Santibáñez, A. Loria, Control of Robot Manipulators in Joint Space, Springer-Verlag, London, UK, 2005.
[21] M.W. Spong, S. Hutchinson, M. Vidyasagar, Robot Modeling and Control, Wiley, New York, USA, 2005.
[22] E. Nuño, I. Sarras, L. Basañez, Consensus in networks of nonidentical Euler–Lagrange systems using P+d controllers, IEEE Trans. Robot. 26 (6) (2013) 1503–1508.
[23] S. Hirche, M. Buss, Human-oriented control for haptic teleoperation, Proc. IEEE 100 (3) (2012) 623–647.
[24] I.G. Polushin, P.X. Liu, C.-H. Lung, Human dynamics and stability of teleoperator systems with generalized projection-based force reflection algorithms, in: 18th IFAC World Congress, Milan, Italy, September 2011, pp. 338–343.
[25] S.F. Atashzar, I.G. Polushin, R.V. Patel, Networked teleoperation with non-passive environment: application to tele-rehabilitation, in: IEEE/RSJ International Conference on Intelligent Robots and Systems, Algarve, Portugal, October 2012, pp. 5125–5130.
[26] A. Mohammadi, M. Tavakoli, A. Jazayeri, PHANSIM: a simulink toolkit for the sensable PHANToM haptic devices, in: 23rd Canadian Congress of Applied Mechanics, Vancouver, BC, Canada, 2011, pp. 787–790.
[27] Y.C. Liu, N. Chopra, Controlled synchronization of heterogeneous robotic manipulators in the task space, IEEE Trans. Robot. 28 (1) (2012) 268–275.
[28] M. Chen, S.S. Ge, B.V.E. How, Robust adaptive neural network control for a class of uncertain mimo nonlinear systems with input nonlinearities, IEEE Trans. Neural Netw. 21 (5) (2010) 796–812.
[29] Y.J. Liu, C.L.P. Chen, G.X. Wen, S. Tong, Adaptive neural output feedback tracking control for a class of uncertain discrete-time nonlinear systems, IEEE Trans. Neural Netw. 22 (7) (2011) 1162–1167.
[30] B. Xu, C. Yang, Z. Shi, Reinforcement learning output feedback nn control using deterministic learning technique, IEEE Trans. Neural Netw. Learn. Syst. 25 (3) (2014) 635–641.
[31] B. Xu, Z. Shi, C. Yang, F. Sun, Composite neural dynamic surface control of a class of uncertain nonlinear systems in strict-feedback form, IEEE Trans. Cybern. (2014) http://dx.doi.org/10.1109/TCYB.2014.2311824.
[32] B. Xu, Z. Shi, C. Yang, S. Wang, Neural hypersonic flight control via time-scale decomposition with throttle setting constraint, Nonlinear Dyn. 73 (3) (2013) 1849–1861.
[33] Y.J. Liu, S. Tong, C.L.P. Chen, Adaptive fuzzy control via observer design for uncertain nonlinear systems with unmodeled dynamics, IEEE Trans. Fuzzy Syst. 21 (2) (2013) 275–288.
[34] C.L.P. Chen, Y.J. Liu, G.X. Wen, Fuzzy neural network-based adaptive control for a class of uncertain nonlinear stochastic systems, IEEE Trans. Cybern. 44 (5) (2014) 583–593.